The solution of vibroacoustic linear systems as a finite sum of transmission paths

Francesc X. Magrans[a], Àngels Aragonès[b], Antonio Rodríguez-Ferran[c], Oriol Guasch[d,*]

[a]*Ingeniería para el Control del Ruido, Berruguete 52, Vila Olímpica (Vall dHebron), 08035 Barcelona, Spain*
[b]*Applus IDIADA, L'Albornar PO Box 20, 43710 Santa Oliva, Spain*
[c]*Laboratori de Càlcul Numèric, Universitat Politècnica de Catalunya Jordi Girona 1, Campus Nord, 08034 Barcelona, Spain*
[d]*GTM - Grup de Recerca en Tecnologies Mèdia, La Salle, Universitat Ramon Llull, C/ Quatre Camins 30, 08022 Barcelona, Catalonia, Spain*

Abstract

Linear systems are frequently encountered in low, mid and high vibroacoustics modelling of mechanical built-up structures. It has recently been proved that the solution to those systems can be always factorized as an *infinite* (weighted) Neumann series summation, which accounts for signal transmission through paths connecting system elements. The key to path expansion relies on the concept of direct transmissibility. In this work, we explore some additional theoretical aspects of transmissibility-based transmission path analysis (TPA), which is known to constitute a valuable tool to remedy noise and vibration problems. In particular, we show that it is also possible to expand the solution of a matrix linear system as a *finite* summation of transmission paths. Furthermore, our goal is to provide mathematical and physical insight into such path factorization. As regards the former, we exploit the relationship between graph theory and matrix algebra to interpret the terms appearing in the series expansion as combinations of open and closed paths in a graph. In what concerns the second, two benchmark examples are addressed that benefit from the graph theory outcomes. The first one consists of a mass-damping-stiffness system representative of vibroacoustic modelling at low frequencies. A relation is established between the relative weights of the paths, the global system resonances and the resonances of complementary systems, which contain elements not belonging to the paths. The second example involves a statistical energy analysis (SEA) model made of connected plates. The meaning of the relative weights of open paths in the finite expansion for energy transmission between SEA subsystems is analyzed and compared to the results of infinite SEA path factorization.

Keywords: Direct transmissibility, Transfer path analysis, Open and closed paths, Vibroacoustic modelling, Neumann series

1. Introduction

Transfer path analysis (TPA) comprises a set of methodologies for inspecting the transmission of structural vibrations and acoustic waves in mechanical systems. The applications of TPA are multiple and usually involve determining the influence of forces entering a buit-up structure on the response at a target degree of freedom (dof), factorizing the response at the target dof in terms of other system dof responses, or resolving the vibroacoustic behaviour of a coupled structure in terms of the vibroacoustic behavior of its individual components. From the multiple and partial coherence analysis in [1–4] and its evolution into operational TPA [5–7], to *classical* force TPA factorization approaches [8–12] and transmissibility methods based on responses [8, 13, 14], a large variety of TPA approaches cohabit nowadays. Rig-based strategies [15], in-situ blocked forces and free velocity techniques [16], and pseudo-force methods [10] can also be viewed as TPA methods. The reader is referred to the very complete review in [17] for an introduction to most of them.

*Corresponding Author: oriol.guasch@salle.url.edu

This work is concerned with some applications of transmissibility-based TPA to general vibroacoustic linear systems. In particular, we are interested in determining whether the response signal at a target dof (or subsystem) can be factorized as a finite summation of path contributions, linking the dof where the external input is applied and the target dof. The key concept to define transmission paths is that of *direct* transmissibility, which was first introduced in [8]. In a nutshell, a direct transmissibility is nothing but the ratio between the responses at two dof when one of them is excited and all other dof in the system remain blocked [8, 18]. Direct transmissbilities gave place to the so called GTDT (Global Transmissibility Direct Transmissibility) TPA method, also known as ATPA (Advanced TPA) in industrial applications. Theoretical works on the GTDT have involved both continuous and discrete systems. In [19], the method was applied to analyze flexural wave propagation in beams, while in [18] a connection was established between direct transmissibilities and the stencils of some finite element and finite difference numerical schemes. Besides, the effects of path blocking were studied in a discrete mass-damping-stiffness system in [19]. Experimental controlled tests to assess the validity of the GTDT have been reported in [20, 21] and industrial applications in the railway sector are described in [22–24]. Direct transmissibilities are also at the basis of an experimental statistical energy analysis (ESEA) approach that does not require measuring external input powers into the system [25], as required in the standard power injection method [26]. Recent developments have concerned the application of the GTDT to the finite element method (FEM) [27], the definition of transmissibilities between groups of subsystems and the introduction of force transmissibilities [28], addressing the problem of structural coupling [29] and facilitating the experimental acquisition of transmissibility functions [30]. Linear systems of equations, on the other hand, appear in a large variety of vibroacoustic problems. At low frequencies, they are encountered, for example, in mechanical systems characterized by a dynamic stiffness matrix and in numerical FEM models as well. In the mid-frequency range, they can describe, for instance, statistical modal energy distribution analysis (SmEdA) [31–33] and energy distribution (ED) models [34], among others. The statistical energy analysis (SEA) method for high frequencies also ends up with a matrix linear system to determine subsystem energies [35–37]. In recent years it has been found that, as mentioned before, the direct transmissibilities introduced in the GTDT method allow one to expand the solution of any matrix linear system in terms of an infinite summation of path contributions. Put another way, the response at any system target dof can be built adding the signal carried out by all infinite paths connecting those dof with external input signal to the target.

The situation is easy to understand in the case of SEA systems where the transmitted variable is energy. Transmission paths in SEA were first recognized in [38]. Soon after that, it was proved in [39] that the subsystem energy vector solving an SEA system admits a Neumann series decomposition whose generating matrix entries consist of direct transmissibilities between subsystems. The n-th power of the generating matrix contains the contributions of groups of n-th order paths to subsystem energies. Nonetheless, this factorization does not provide a sorted classification of transmission paths, which is necessary to remedy vibroacoustic problems (e.g. for reducing the vibration or sound pressure at a receiver subsystem). In this sense, one step forward was carried out in [40] by establishing a formal connection between SEA and graph theory. The generating matrix of the development in [39] was identified in [40] with the adjacency matrix of a graph. This permitted exploiting powerful graph theory algorithms to classify dominant paths in SEA models in a very fast an efficient way [41, 42]. Such algorithms have been latterly applied to analyze vibration problems in naval structures [43, 44]. Graph cut algorithms have been also proposed to mitigate energy transmission in SEA models [45]. Furthermore, it is worthwhile noting that bond graph theory has been recently applied to TPA [46, 47].

The basic premise for a proper system path factorization is that the infinite series expansion converges. This can be proved without much difficulty in SEA (see e.g., [39, 41, 37] for different alternatives) but turns out to be more difficult for mid and low frequency vibroacoustic linear systems. The decomposition was demonstrated to be feasible for SmEdA models in [48] and with some restrictions for ED models in [49]. A more general result which somewhat encompasses all previous ones has been recently proved in [50]. If the terms in the Neumann series are properly weighted, path factorization is possible for any system of linear equations. This means that regardless of the linear vibroacoustic system we have (low, mid or high frequency models), its solution can always be expressed in terms of paths. Admittedly, though, while paths have an easy physical interpretation for mid to high frequency models (e.g. in SmEdA and SEA), their meaning is

not so clear for low frequency models.

All the above cited works contemplate the system solution expansion in terms of an *infinite* number of paths, with independence of the dimension of the analyzed system. In practice, the latter will be almost always finite even for continuous complex structures (note that discrete numerical approximations are often employed to simulate them). This means that paths connecting two different dof always contain cycles. In this work, we wonder whether it is possible to factorize the solution of any linear vibroacoustic system by way of a *finite* set of properly weighted *open* paths (i.e. without cycles), instead of an infinite one. More specifically, for a system characterized with n degrees of freedom, only paths of order up to $n-1$ shall be required. It is shown in the paper that such factorization is viable and its mathematical and physical meanings are investigated. Concerning the former, the connection with graph theory is exploited and the different components of the Leibniz formula for a matrix determinant are interpreted in terms of loops, closed and open paths in a graph. As regards the physical meaning, the finite open path factorization is implemented for two benchmark problems: a low frequency mass-damping-stiffness mechanical system and a high frequency SEA model. Physical explanations are attempted for the weights in their respective series developments.

The outline of the remainder of this manuscript is as follows. The basic problem is introduced in section 2. Section 3 is devoted to factorize the inverse of a matrix as a finite sum of paths in a graph representing the analyzed vibroacoustic system. The two illustrative examples typifying low and high frequency vibroacoustic models are presented in section 4. The graph theory results of section 3 are applied to them and the different physical interpretation of path weights is highlighted for both cases. Remarks on dissimilarities with infinite series factorization are also reported. Conclusions close the paper in section 5.

2. Problem statement

Let us consider the linear matrix system

$$\mathbf{A}\mathbf{x} = \mathbf{b} \tag{1}$$

in which $\mathbf{A}$ is an invertible real or complex $n \times n$ matrix, $\mathbf{x}$ an $n \times 1$ vector of unknowns and $\mathbf{b}$ an $n \times 1$ constant vector. As said in the Introduction, the system in Eq. (1) can represent many different problems in vibroacoustics. For instance, at high frequencies it could stand for an SEA model in which $\mathbf{A}$ denotes the matrix of loss factors, $\mathbf{x}$ the subsystem energy vector and $\mathbf{b}$ the external power per radian frequency, input into the system. In the mid-frequency range, Eq. (1) could be an energy distribution model with $\mathbf{A}$ being now the inverse of an influence energy coefficient matrix, $\mathbf{x}$ standing again for the vector of subsystem energies and $\mathbf{b}$ for the external input power. Alternatively, in SmEdA Eq. (1) would involve a matrix of modal loss factors, an unknown vector of modal energies and a constant vector of external input modal power. Besides, at low frequencies the system matrix would typically correspond to a dynamic stiffness e.g., $\mathbf{A} = (-\omega^2\mathbf{M} + \mathbf{K})$, with ω being the radian frequency, $\mathbf{M}$ a real mass matrix and $\mathbf{K}$ a complex stiffness matrix, in the particular case of a system with structural damping. The entries of $\mathbf{x}$ would be the d.o.f displacements and $\mathbf{b}$ would represent an external force vector. The system matrix could be built either from experimental results, numerical modelling (e.g., using FEM) or derived from analytical developments.

The system in Eq. (1) can be straightforwardly solved by means of an appropriate direct (i.e. Gaussian) or iterative (i.e. Krylov) solver. However, in practice this provides little, if any, information on the underlying physics of Eq. (1). Therefore, other options are favoured. In the low frequency regime, one would typically resort to a modal decomposition of the solution $\mathbf{x}$. Another option consists in factorizing the response $\mathbf{x}$ in terms of the transmission paths that the external inputs follow from a system entrance point to a receiver one. For example, in SEA the energy at any receiver subsystem can be expressed adding the contributions of all energy transmission paths connecting a source subsystem (where external energy is input) with the receiver one. As cycles are permitted, there exist an infinite amount of paths. In SEA though, the longer the path the less the contribution so in practice the susbsystem energies can be approximately well recovered from a finite set of dominant transmission paths [41].

To decompose the solution of Eq. (1) in terms of paths it becomes necessary to introduce a *transmissibility* matrix $\mathbf{T}$ (see [50]), such that

$$\mathbf{T} = -\mathbf{D}^{-1}(\mathbf{L} + \mathbf{U}), \tag{2}$$

where $\mathbf{D} = \mathrm{diag}(\mathbf{A})$ is assumed to be invertible, and $\mathbf{L}$ and $\mathbf{U}$ are the strict lower and upper triangular matrices of $\mathbf{A}$. It shall be noted that the off-diagonal entries of $\mathbf{T}$ are exactly those of the direct transmissibility matrix defined in [8, 18]. The only difference is that $\mathbf{T}$ contains zeros in its diagonal. Given that $\mathbf{A} = \mathbf{D} + \mathbf{L} + \mathbf{U}$, it is clear that $\mathbf{A} = \mathbf{D}(\mathbf{I} - \mathbf{T})$ so the solution to Eq. (1) can be expressed as

$$\mathbf{x} = (\mathbf{I} - \mathbf{T})^{-1}\mathbf{D}^{-1}\mathbf{b}. \tag{3}$$

The key to path factorization consists in expressing $(\mathbf{I}-\mathbf{T})^{-1}$ as a summation of powers of $\mathbf{T}$. Whenever the spectral radius of $\mathbf{T}$ is less than unity, $\rho(\mathbf{T}) < 1$, the inverse $(\mathbf{I}-\mathbf{T})^{-1}$ can be expanded as a convergent Neumann series,

$$(\mathbf{I} - \mathbf{T})^{-1} = \sum_{k=0}^{\infty} \mathbf{T}^k. \tag{4}$$

As mentioned before, in vibroacoustics it has already been proved that SEA systems admit such type of development [39, 41, 37]. This was also proven for SmEdA [48] and for some ED models as well [49]. More recently, it has been demonstrated that expressing $(\mathbf{I}-\mathbf{T})^{-1}$ in terms of modified Neumann series is in fact always possible, even if $\rho(\mathbf{T}) > 1$ [50]. In this case, the main difference with Eq. (4) is that the powers of $\mathbf{T}$ beyond a certain value of k need to be appropriately weighted.

For mid-high frequency vibroacoustic models, an expansion like Eq. (4) has a clear physical meaning in terms of transmission of energy through paths connecting subsystems [39, 41], or connecting individual modes belonging to different subsystems [48]. As mentioned in the Introduction, this has opened the door to potential practical applications to mitigate noise and vibration problems. Unfortunately, the physical interpretation of the series is not so clear in the case of low frequency models for which $\rho(\mathbf{T}) > 1$, though the underlying concept of direct transmissibility in the entries of $\mathbf{T}$ is totally valid and lies at the basis of widely employed TPA methods in vibroacoustics.

The Neumann series in Eq. (4) and its modified analogous for $\rho(\mathbf{T}) > 1$ involve an infinite number of terms. In the next sections, we provide an alternative expansion to Eq. (4) for the system solution in Eq. (3). The main difference is that the proposed factorization only involves a finite number of paths instead of an infinite one. The general vibroacoustic linear system in Eq. (1) is considered with independence of the value of its spectral radius. The results therefore apply to low, mid and high frequency vibroacoustic models. Both a mathematical interpretation of the finite expansion in the framework of graph theory and a physical one are suggested.

3. The inverse of a matrix as a finite sum of paths

3.1. Relation between the entries of matrix $\mathbf{B}$ *and the entries of its adjugate matrix* $\mathbf{B}_{[ji]}$

Let $\mathbf{B} \in \mathbb{C}^{n\times n}$ (for damped systems) or $\mathbb{R}^{n\times n}$ (for undamped systems) be an invertible matrix. It may be regarded as a weighted directed digraph, see Fig. 1: the off-diagonal entries b_{ij} with $i \neq j$ represent the directed (i, j)-arcs, whereas the diagonal entries b_{ii} represent loops.

The inverse of matrix $\mathbf{B}$ may be computed by means of the *adjugate matrix* (i.e. transpose matrix of cofactors) as

$$\mathbf{B}^{-1} = \mathrm{adj}(\mathbf{B}) / \det(\mathbf{B}) \tag{5}$$

with

$$\mathrm{adj}(\mathbf{B}) = \left((-1)^{i+j} M_{ji}\right)_{1\leq i,j\leq n} \tag{6}$$

where M_{ji} is the (j, i)-minor of $\mathbf{B}$ (that is, the determinant of matrix $\mathbf{B}_{[ji]} \in \mathbb{R}^{(n-1)\times(n-1)}$ that results from

$$\mathbf{B} = \begin{bmatrix} b_{11} & b_{12} & b_{13} & b_{14} \\ b_{21} & b_{22} & b_{23} & b_{24} \\ b_{31} & b_{32} & b_{33} & b_{34} \\ b_{41} & b_{42} & b_{43} & b_{44} \end{bmatrix}$$

(a)

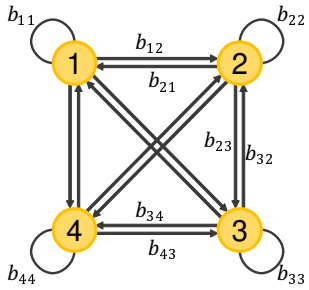

(b)

Figure 1: Matrices and graphs: (a) a matrix of dimension $n = 4$; (b) associated weighted graph.

deleting row j and column i of matrix $\mathbf{B}$):

$$\mathbf{B}_{[ji]} = \begin{bmatrix} b_{11} & \cdots & b_{1,i-1} & b_{1,i+1} & \cdots & \cdots & \cdots & \cdots & b_{1n} \\ \vdots & \ddots & \vdots & \vdots & & & & & \vdots \\ b_{i-1,1} & \cdots & b_{i-1,i-1} & \vdots & & & & & \vdots \\ \vdots & & \vdots & b_{i,i+1} & & & & & \vdots \\ \vdots & & \vdots & & \ddots & & & & \vdots \\ b_{j-1,1} & \cdots & b_{j-1,i-1} & & & b_{j-1,j} & & & b_{j-1,n} \\ b_{j+1,1} & \cdots & b_{j+1,i-1} & & & & b_{j+1,j+1} & \cdots & b_{j+1,n} \\ \vdots & & \vdots & & & & \vdots & \ddots & \vdots \\ b_{n1} & \cdots & b_{n,i-1} & \cdots & \cdots & \cdots & b_{n,j+1} & \cdots & b_{nn} \end{bmatrix} \tag{7}$$

Note that, for $j \neq i$, some of the diagonal entries of $\mathbf{B}_{[ji]}$ are not diagonal entries of $\mathbf{B}$. For the case $j > i$ illustrated in Eq. (7), the diagonal entries of $\mathbf{B}_{[ji]}$ are

$$b_{pp} \quad \text{for} \quad p = 1, \ldots, i-1, j+1, \ldots, n \quad ; \quad b_{p,p+1} \quad \text{for} \quad p = i, \ldots, j-1 \tag{8}$$

More generally, the entries of matrices $\mathbf{B}$ and $\mathbf{B}_{[ji]}$ are related by

$$(b_{[ji]})_{PQ} = b_{pq} \tag{9}$$

with subscripts PQ connected to pq by

$$P = \begin{cases} p & \text{for} \quad p = 1, \ldots, j-1 \\ p-1 & \text{for} \quad p = j+1, \ldots, n \end{cases} \quad ; \quad Q = \begin{cases} q & \text{for} \quad q = 1, \ldots, i-1 \\ q-1 & \text{for} \quad q = i+1, \ldots, n \end{cases} \tag{10}$$

or, inversely,

$$p = \begin{cases} P & \text{for} \quad P = 1, \ldots, j-1 \\ P+1 & \text{for} \quad P = j, \ldots, n-1 \end{cases} \quad ; \quad q = \begin{cases} Q & \text{for} \quad Q = 1, \ldots, i-1 \\ Q+1 & \text{for} \quad Q = i, \ldots, n-1 \end{cases} . \tag{11}$$

3.2. Determinant of matrix $\mathbf{B}$

The determinant of matrix $\mathbf{B}$ is expressed by Leibniz formula as

$$\det(\mathbf{B}) = \sum_{\tau \in S_n} \operatorname{sgn}(\tau) \prod_{i \in \mathbb{N}_n} b_{i,\tau(i)} \tag{12}$$

where S_n is the set of all permutations τ of $\mathbb{N}_n = \{1, 2, \ldots, n\}$ and sgn is the sign operator. We will now explore the summands in Eq. (12).

3.2.1. Case with no loops

Let us consider first a permutation such that $\tau(i) \neq i$ for all $i \in \mathbb{N}_n$. Then $\prod_{i\in\mathbb{N}_n} b_{i,\tau(i)}$ is the weight of a directed path with the following properties:

- order n (because it contains n arcs)
- no loops (because there are no diagonal entries b_{ii})
- all nodes are the tail and the head of exactly one directed arc (because i spans $\mathbb{N}_n$ and τ is a permutation)

With these conditions, $\prod_{i\in\mathbb{N}_n} b_{i,\tau(i)}$ is necessarily one cycle (i.e. closed path) or a disjoint union of cycles[1], see Fig. 2. No open paths are possible.

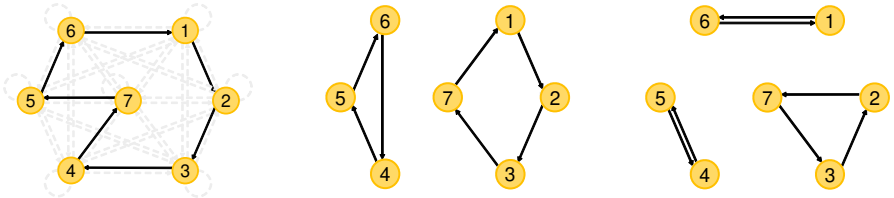

Figure 2: Case with no loops: if the permutation $\tau \in S_n$ moves all indices, then $\prod_{i\in\mathbb{N}_n} b_{i,\tau(i)}$ represents either (a) one cycle or (b-c) a disjoint union of cycles.

3.2.2. Case with loops

Let us assume now that the permutation τ verifies $\tau(i) = i$ for all $i \in \mathbb{F}$, a subset of $\mathbb{N}_n$ with f elements. Note that the two extreme cases are $\mathbb{F} = \emptyset$, $f = 0$ (as assumed in section 3.2.1) and $\mathbb{F} \equiv \mathbb{N}_n$, $f = n$. Intermediate cases correspond to $f = 1, \ldots, n-2$ (but not $f = n-1$). Let us explore one such intermediate case:

$$\prod_{i\in\mathbb{N}_n} b_{i,\tau(i)} = \prod_{i\in\mathbb{F}} b_{ii} \prod_{i\notin\mathbb{F}} b_{i,\tau(i)} \tag{13}$$

The first product in the right-hand-side of Eq. (13) represents f loops, see Fig. 3. The second product represents a directed path of order $n-f$ consisting of one cycle or a disjoint union of cycles. Again, no open paths are present.

3.3. Determinant of the adjugate matrix $\mathbf{B}_{[ji]}$

According to Leibniz formula,

$$M_{ji} \equiv \det(\mathbf{B}_{[ji]}) = \sum_{\tau\in S_{n-1}} \operatorname{sgn}(\tau) \prod_{P\in\mathbb{N}_{n-1}} (b_{[ji]})_{P,\tau(P)} \tag{14}$$

Note that S_{n-1} is the set of all permutations of $\mathbb{N}_{n-1} = \{1, 2, \ldots, n-1\}$. Let us explore the summands in Eq. (14).

[1] Or, more precisely, the weight of one cycle or a disjoint union of cycles; we will omit "weight" for brevity in the remainder.

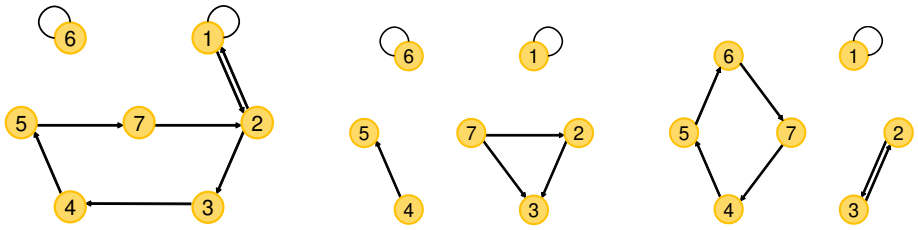

Figure 3: Case with loops: if the permutation $\tau \in S_n$ leaves f indices fixed, then $\prod_{i\in\mathbb{N}_n} b_{i,\tau(i)}$ contains f loops and (a) one cycle or (b-c) a disjoint union of cycles.

3.3.1. Case with no loops

Consider a permutation $\tau \in S_{n-1}$ such that $p(P) \neq q(\tau(P))$ for all $P \in \mathbb{N}_{n-1}$. This means that the product $\prod_{P\in\mathbb{N}_{n-1}} (b_{[ji]})_{P,\tau(P)}$ contains no diagonal terms of matrix $\mathbf{B}$. The associated directed path has the following properties:

- order $n-1$
- no loops
- all nodes are the tail of exactly one directed arc except node j, because $p(P)$ does not take value j
- all nodes are the head of exactly one directed arc except node i, because $q(\tau(P))$ does not take value i

With these conditions, the path consists of an open directed path of order m (with $m = 1, \ldots, n-1$) that starts at node i and ends at node j, and a cycle or a disjoint union of cycles with a total of $(n-1)-m$ arcs[2], see Fig. 4.

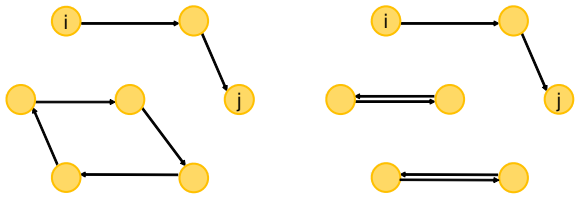

Figure 4: If the graph $\prod_{P\in\mathbb{N}_{n-1}} (b_{[ji]})_{P,\tau(P)}$ contains no loops, it consists of one open directed path with the tail in node i and the head in node j, and (a) one cycle or (b) a disjoint union of cycles.

3.3.2. Case with loops

Let us assume now that the permutation $\tau \in S_{n-1}$ verifies $p(P) = q(\tau(P))$ for all $P \in \mathbb{F}$, a subset of $\mathbb{N}_{n-1}$ with f elements. Then

$$\prod_{P\in\mathbb{N}_{n-1}} (b_{[ji]})_{P,\tau(P)} = \prod_{P\in\mathbb{F}} b_{p(P),p(P)} \prod_{P\notin\mathbb{F}} b_{p(P),q(\tau(P))} \tag{15}$$

[2]Except for $i = j$. In this case, the path is a cycle or a disjoint union of cycles with a total of $(n-1)$ arcs.

As discussed above in sections 3.2.2 and 3.3.1, the first product in the right-hand-side of Eq. (15) represents f loops, whereas the second product represents one open directed path connecting nodes i and j, and cycle(s) connecting all remaining nodes[3], see Fig. 12.

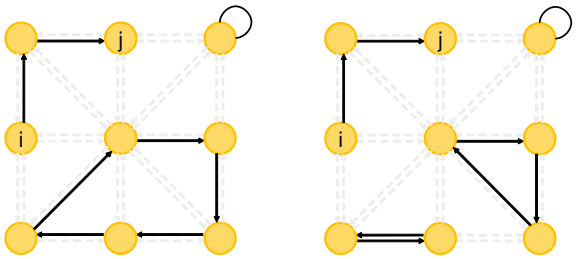

(a) (b)

Figure 5: In the general case, the path $\prod_{P\in\mathbb{N}_{n-1}}(b_{[ji]})_{P,\tau(P)}$ contains f loops, an open path of order m that connects nodes i and j, and cycle(s) with a total of $(n-1)-f-m$ arcs.

3.4. Open paths are weighted by complementary cycles

The solution of a linear system by means of the transmissibility matrix $\mathbf{T}$ requires the computation of the inverse of matrix $\mathbf{I}-\mathbf{T}$, see Eq. (3). Taking $\mathbf{B}=\mathbf{I}-\mathbf{T}$ results in $b_{ii}=1$ for $i=1,\ldots,n$ (that is, the loops in figures 3 and 12 have weight 1) and $b_{ij}=-t_{ij}$ for $i\neq j$. A careful inspection of the resulting expression reveals that the cofactors of Eq. (6) can be expressed as

$$(-1)^{i+j}M_{ji}=\sum_{k=1}^{n-1}\sum_{l=1}^{n_k}\overbrace{\prod_{P\in\mathbb{N}_{\text{open},l}}(t_{[ji]})_{P,\tau_l(P)}}^{\text{open path}}\overbrace{\det\left((\mathbf{I}-\mathbf{T})_{[ji]_{\mathbb{N}_{\text{comp},l}\times\mathbb{N}_{\text{comp},l}}}\right)}^{\text{complementary subsystem}} \tag{16}$$

In Eq. (16), all the permutations in Eq. (14) have been grouped according to their open path. Index k denotes the order of the open path, and ranges from 1 (that is, the (i,j)-arc) to $n-1$ (that is, open paths that visit all nodes in the graph). Index l is a counter of open paths of order k; a simple combinatorics exercise shows that the number of open paths of order k that connect nodes i and j is $n_k=(n-2)!/(n-1-k)!$. For each open path l of order k, we consider a partition $\mathbb{N}_{n-1}=\mathbb{N}_{\text{open},l}\cup\mathbb{N}_{\text{comp},l}$, where $\mathbb{N}_{\text{open},l}$ is a subset of k integers (i.e. the tail numbers of the arcs in the open path) and $\mathbb{N}_{\text{comp},l}$ is the complementary subset. Eq. (16) shows that each open path is *weighted* by the determinant of the complementary subsystem. This determinant accounts for all possible cycles that complement that particular open path.

Finally, by dividing Eq. (16) by $\det(\mathbf{I}-\mathbf{T})$, according to Eq. (5), one gets

$$\left[(\mathbf{I}-\mathbf{T})^{-1}\right]_{ij}=\frac{(-1)^{i+j}M_{ji}}{\det(\mathbf{I}-\mathbf{T})}= \sum_{\text{open paths}}\text{(weight of open path)}\times\text{(relative weight of complementary subsystem)} \tag{17}$$

Eq. (17) shows that the entry ij of matrix $(\mathbf{I}-\mathbf{T})^{-1}$ is a weighted sum of all the (weights of) open paths that connect nodes i and j. Each open path is weighted by the ratio of (the weights of) the cycles of the complementary subsystem over (the weights of) the cycles of the overall system. As regards the latter, it is to be mentioned that as $\mathbf{T}$ has zeros on the diagonal it can be identified with the weighted adjacency matrix of a directed graph and it is a well-known result in graph theory that $\det(\mathbf{I}-\mathbf{T})$ can be expanded as the summation of the weights of all cycles in the graph (see [51, 52]; note this is still a topic of some research in graph theory e.g., [53, 54]).

[3]Except for $i=j$. In this case, the path contains f loops and cycle(s) connecting all remaining $(n-1)-f$ nodes.

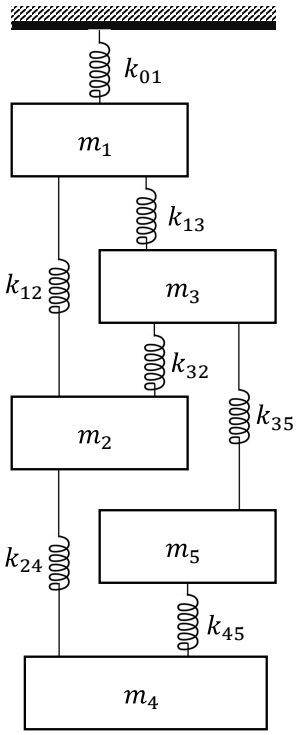

Figure 6: 5 dof mechanical system with structural damping.

4. Physical interpretation and illustrative examples

In the previous section, we have shown that Eq. (17) has a clear geometrical interpretation in the framework of graph theory. In this section, we would also like to provide a certain physical meaning for it. We believe the best way to do so is by means of some examples. Two of them will be considered. The first one consists of a mass-damping-stiffness mechanical system, which typifies low frequency vibroacoustic problems. The second one deals with high frequency vibroacoustics modelling and involves an SEA system.

4.1. First example: a 5 dof mass-damping-stiffness mechanical system

4.1.1. Model description

Let us first address the case of a mechanical system with structural damping, which is made of five masses $m_i,\ i = 1 \ldots 5$, linked by springs of complex stiffness k_{ij}, according to the configuration in Fig. 6. The values of m_i and k_{ij} are collected in Table 1. The dynamic stiffness matrix $\mathbf{A} = (-\omega^2\mathbf{M} + \mathbf{K})$ can be built as usual from the values of m_i and k_{ij}, with $\mathbf{M} \in \mathbb{R}^{5\times5}$ and $\mathbf{K} \in \mathbb{C}^{5\times5}$. Furthermore, in section 2 we have seen that $\mathbf{A} = \mathbf{D}(\mathbf{I} - \mathbf{T})$, which allows one to obtain the transmissibility matrix $\mathbf{T}$ as

$$\mathbf{T}(\omega) = \mathbf{I} - \mathbf{D}^{-1}(-\omega^2\mathbf{M} + \mathbf{K}). \tag{18}$$

Note that we have explicitly indicated the dependence of $\mathbf{T} \in \mathbb{C}^{5\times5}$ with the radian frequency ω for the sake of clarity in forthcoming explanations.

4.1.2. Relation between the mechanical resonances of the dynamic stiffness matrix and the eigenvalues of $\mathbf{T}$

Before starting the transmission path analysis of the system in Fig. 6, we elaborate a little bit on the relation between the resonances of a mechanical system with structural damping and the eigensolutions

Table 1: Mass and stiffness values for the discrete system in Fig. 6.

Mass (kg)	Stiffness (N/m)
$m_1 = 0.15$	$k_{01} = 1 \times 10^5(1 + \mathrm{i}0.05)$
$m_2 = 0.13$	$k_{12} = 2 \times 10^5(1 + \mathrm{i}0.05)$
$m_3 = 0.15$	$k_{13} = 5 \times 10^5(1 + \mathrm{i}0.05)$
$m_4 = 0.13$	$k_{24} = 3 \times 10^4(1 + \mathrm{i}0.05)$
$m_5 = 0.17$	$k_{32} = 3 \times 10^5(1 + \mathrm{i}0.05)$
	$k_{35} = 2 \times 10^5(1 + \mathrm{i}0.05)$
	$k_{45} = 5 \times 10^5(1 + \mathrm{i}0.05)$

of the transmissibility matrix $\mathbf{T}$. Unless specified, the herafter reported results will be valid for a general system with $\mathbf{A} \in \mathbb{C}^{n\times n}$, $n = 5$ being a particular case. Taking $\mathbf{b} = \mathbf{0}$ in Eq. (1) and $\mathbf{A} = (-\omega^2\mathbf{M} + \mathbf{K})$ yields the generalized eigenvalue problem

$$(-\omega^2\mathbf{M} + \mathbf{K})\mathbf{x} = \mathbf{0}, \tag{19}$$

with solution eigenpairs $(\omega_i^2, \mathbf{\Psi}_i)$ ($\omega_i^2 \in \mathbb{C}$, $\mathbf{\Psi}_i \in \mathbb{C}^{n\times 1}$) satisfying $(-\omega_i^2\mathbf{M} + \mathbf{K})\mathbf{\Psi}_i = \mathbf{0}$. The resonances of the mechanical system take place at ω_i and the modal shapes are given by $\mathbf{\Psi}_i$. On the other hand, suppose that $(\lambda_k, \mathbf{\Phi}_k)$ are eigenpairs of $\mathbf{T}$, i.e.,

$$\mathbf{T}(\omega)\mathbf{\Phi}_k = \lambda_k\mathbf{\Phi}_k, \tag{20}$$

with $\lambda_k(\omega) \in \mathbb{C}$ and $\mathbf{\Phi}_k(\omega) \in \mathbb{C}^{n\times 1}$, both depending on ω. If we next evaluate $\mathbf{T}$ at the system resonance ω_i and take the product with its corresponding modal shape vector $\mathbf{\Psi}_i$, we get

$$\mathbf{T}(\omega_i)\mathbf{\Psi}_i = [\mathbf{I} - \mathbf{D}^{-1}(-\omega_i^2\mathbf{M} + \mathbf{K})]\mathbf{\Psi}_i = \mathbf{\Psi}_i. \tag{21}$$

This means that the system modal shape vector $\mathbf{\Psi}_i$ is also an eigenvector of $\mathbf{T}(\omega_i)$, i.e., $\mathbf{\Psi}_i \equiv \mathbf{\Phi}_k$ with eigenvalue λ_k such that $\mathrm{Re}(\lambda_k) = 1$ and $\mathrm{Im}(\lambda_k) = 0$.

We can check this assertion for our particular five-dimensional problem in Fig. 6, which has the complex resonances $f_{A,i} = \omega_i/2\pi$ in Table 2. In Fig. 7, we present five subplots exploring the complex plane for $\omega \in \mathbb{C}$ such that $\mathrm{Re}(\omega) \geq 0 \wedge \mathrm{Im}(\omega) \geq 0$, to locate where the complex eigenvalues of $\mathbf{T}$ match the system mechanical resonances. Let us first focus on the top left subplot. This contains five red squares which indicate the resonance values of Table 2, in the complex plane. For every frequency value $\omega \in \mathbb{C}$ in the figure, we compute the first eigenvalue $\lambda_1(\omega)$ of $\mathbf{T}(\omega)$, using a resolution of 0.11 Hz in the real axis and 0.013 units in the imaginary one. If $1 - \varepsilon_{\mathrm{Re}} \leq \mathrm{Re}(\lambda_1(\omega)) \leq 1 + \varepsilon_{\mathrm{Re}}$ a blue dot is plotted for $f = \omega/2\pi$ in the plane. Here, $\varepsilon_{\mathrm{Re}}$ is a predetermined tolerance value that has been taken as $\varepsilon_{\mathrm{Re}} = 5 \times 10^{-3}$ for a better visualization of the curves in the figure (smaller values can be used for better accuracy). Likewise, if $-\varepsilon_{\mathrm{Im}} \leq \mathrm{Im}(\lambda_1(\omega)) \leq \varepsilon_{\mathrm{Im}}$ (with $\varepsilon_{\mathrm{Im}} = 10^{-4}$), we plot a yellow dot in the figure. The value of ω at which both conditions are satisfied corresponds to the first mechanical resonance of the system (i.e., $\omega = \omega_1$) so the blue and yellow curves cross at $f_{A,1} = \omega_1/2\pi$, as observed in the figure and predicted from Eq. (21). The other four subfigures in Fig. 7 present akin results for the other four eigenvalues of $\mathbf{T}$, namely $\lambda_2(\omega)$, $\lambda_3(\omega)$, $\lambda_4(\omega)$ and $\lambda_5(\omega)$. It is to be noted that similar results would have been obtained if considering other dynamic stiffness matrices or numerical models for $\mathbf{A}$, instead that of structural damping.

4.1.3. Solution in terms of transmission paths

Let us next focus on the path analysis and therefore on matrix $(\mathbf{I} - \mathbf{T})^{-1}$. As demonstrated in section 3, any entry ij of this matrix can be decomposed as a weighted finite sum of open paths connecting i with j

Table 2: Complex resonance frequencies for the mass-damping-stiffness system in Fig. 6.

$f_{A,1}$	$f_{A,2}$	$f_{A,3}$	$f_{A,4}$	$f_{A,5}$
$54.73 + 1.36\mathrm{i}$	$181.98 + 4.39\mathrm{i}$	$381.89 + 9.15\mathrm{i}$	$438.81 + 2.2\mathrm{i}$	$499.15 + 11.5\mathrm{i}$

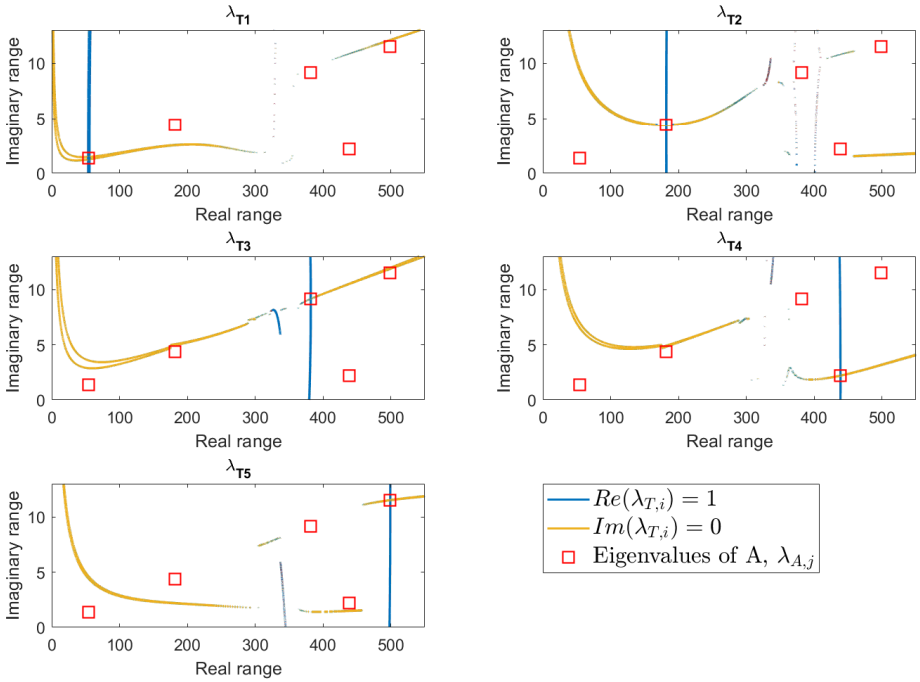

Figure 7: Finding the matching between eigenvalues of $\mathbf{T}$ and system resonances in the complex plane. Each subplot corresponds to one eigenvalue of $\mathbf{T}$. The blue lines indicate eigenvalues of $\mathbf{T}$ with real part close to one while yellow lines indicate eigenvalues of $\mathbf{T}$ with imaginary part close to zero. When both conditions are met the mechanical system resonances in Table 2 are recovered (red squares).

and we would like to figure out its physical meaning for the mass-damping-stiffness example at hand. The graph associated to the transmissibility matrix $\mathbf{T}$ is shown in Fig. 8, the arcs being represented by grey lines. Please note that no lines are drawn between masses that are not physically connected and would therefore have an arc with zero weight. Our goal is to apply the factorization of Eq. (17) in terms of open paths to one of the elements of matrix $\mathbf{T}$. Before proceeding, however, we shall introduce some notation. In forthcoming expressions, $\mathbf{T}_{\{ijk\}}$ will designate the square block matrix of $\mathbf{T}$ made of rows i, j, k and columns i, j, k. For instance, $\mathbf{T}_{\{345\}}$ is the 3 dof mass-damping-stiffness system built suppressing rows and columns 1 and 2 from $\mathbf{T}$. Moreover, we will denote by $\lambda_{m\{ijk\}}$ the m-th eigenvalue of $\mathbf{T}_{\{ijk\}}$.

If we were to apply Eq. (17) to, say, the $i = 2$, $j = 1$ element of $(\mathbf{I} - \mathbf{T})^{-1}$, namely, $(\mathbf{I} - \mathbf{T})^{-1}_{21}$, and assume that all masses were connected to each other (i.e. the graph in Fig. 8 was a complete digraph with

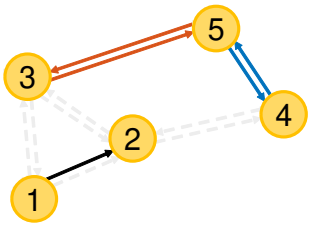

Figure 8: Graph of the 5 dof mechanical system. Closed paths $t_{35}t_{53}$ and $t_{45}t_{54}$ weighting the open path t_{12}.

no missing grey lines), we would get

$$\begin{aligned}
[(\mathbf{I}-\mathbf{T})^{-\mathbf{1}}]_{(2,1)} &= \sum_{\text{open paths}} \text{(weight of open path)} \times \text{(relative weight of complementary subsystem)} \\
&= \frac{1}{\det(\mathbf{I}-\mathbf{T})}\{t_{21}(1-t_{34}t_{43}-t_{45}t_{54}-t_{35}t_{53}-t_{34}t_{45}t_{53}-t_{35}t_{43}t_{54}) \\
&+ t_{23}t_{31}(1-t_{45}t_{54}) \\
&+ t_{24}t_{41}(1-t_{35}t_{53}) \\
&+ t_{25}t_{51}(1-t_{34}t_{43}) \\
&+ t_{23}t_{34}t_{41}+t_{24}t_{43}t_{31}+t_{23}t_{35}t_{51}+t_{25}t_{53}t_{31}+t_{24}t_{45}t_{51} \\
&+ t_{25}t_{54}t_{41}+t_{23}t_{34}t_{45}t_{51}+t_{23}t_{35}t_{54}t_{41}+t_{24}t_{45}t_{53}t_{31} \\
&+ t_{24}t_{43}t_{35}t_{51}+t_{25}t_{54}t_{43}t_{31}+t_{25}t_{53}t_{34}t_{41}\},
\end{aligned} \tag{22}$$

which can be rewritten as

$$\begin{aligned}
[(\mathbf{I}-\mathbf{T})^{-\mathbf{1}}]_{(2,1)} &= \frac{\det(\mathbf{I}-\mathbf{T}_{\{345\}})}{\det(\mathbf{I}-\mathbf{T})}t_{21} \\
&+ \frac{\det(\mathbf{I}-\mathbf{T}_{\{45\}})}{\det(\mathbf{I}-\mathbf{T})}t_{23}t_{31}+\frac{\det(\mathbf{I}-\mathbf{T}_{\{35\}})}{\det(\mathbf{I}-\mathbf{T})}t_{24}t_{41}+\frac{\det(\mathbf{I}-\mathbf{T}_{\{34\}})}{\det(\mathbf{I}-\mathbf{T})}t_{25}t_{51} \\
&+ \frac{1}{\det(\mathbf{I}-\mathbf{T})}t_{23}t_{34}t_{41}+\frac{1}{\det(\mathbf{I}-\mathbf{T})}t_{24}t_{43}t_{31}+\frac{1}{\det(\mathbf{I}-\mathbf{T})}t_{23}t_{35}t_{51} \\
&+ \frac{1}{\det(\mathbf{I}-\mathbf{T})}t_{25}t_{53}t_{31}+\frac{1}{\det(\mathbf{I}-\mathbf{T})}t_{24}t_{45}t_{51}+\frac{1}{\det(\mathbf{I}-\mathbf{T})}t_{25}t_{54}t_{41} \\
&+ \frac{1}{\det(\mathbf{I}-\mathbf{T})}t_{23}t_{34}t_{45}t_{51}+\frac{1}{\det(\mathbf{I}-\mathbf{T})}t_{23}t_{35}t_{54}t_{41} \\
&+ \frac{1}{\det(\mathbf{I}-\mathbf{T})}t_{24}t_{45}t_{53}t_{31}+\frac{1}{\det(\mathbf{I}-\mathbf{T})}t_{24}t_{43}t_{35}t_{51} \\
&+ \frac{1}{\det(\mathbf{I}-\mathbf{T})}t_{25}t_{54}t_{43}t_{31}+\frac{1}{\det(\mathbf{I}-\mathbf{T})}t_{25}t_{53}t_{34}t_{41}.
\end{aligned} \tag{23}$$

Note that Eq. (23) has been expressed in such a way that the first line in the equation contains the weighted contribution of the direct link between masses m_1 and m_2, i.e. the first order path between them. The second line contains the weighted contributions of second order paths linking m_1 and m_2. Likewise, lines third and fourth account for the third order paths and lines five to seven for the fourth order paths, which involve all masses in the system. Nonetheless, in our model of Fig. 6 with graph in Fig. 8 not every mass is linked to all other masses, and one can appreciate that $t_{14} = t_{41} = t_{15} = t_{51} = t_{25} = t_{52} = t_{34} = t_{43} = 0$.

Consequently, Eq. (23) strongly simplifies to

$$\begin{aligned}[(\mathbf{I}-\mathbf{T})^{-\mathbf{1}}]_{(2,1)} = &\frac{\det(\mathbf{I}-\mathbf{T}_{\{345\}})}{\det(\mathbf{I}-\mathbf{T})}t_{21} \\ &+ \frac{\det(\mathbf{I}-\mathbf{T}_{\{45\}})}{\det(\mathbf{I}-\mathbf{T})}t_{23}t_{31} \\ &+ \frac{1}{\det(\mathbf{I}-\mathbf{T})}t_{24}t_{45}t_{53}t_{31}.\end{aligned} \tag{24}$$

with $\det(\mathbf{I}-\mathbf{T}_{\{345\}}) = (1 - t_{45}t_{54} - t_{35}t_{53})$. For illustrative purposes, in Fig. 8 we have plotted the two closed paths with weights $t_{45}t_{54}$ and $t_{35}t_{53}$ (see first line in Eq. (24) and the blue and orange arrows in the figure) affecting the relative weight of the first order open path from m_2 to m_1 (black line in the figure).

A close inspection of the relative weights in the paths of Eq. (23) (and/or the particular case in Eq. (24)) reveals their physical meaning. All paths share the same denominator $\det(\mathbf{I}-\mathbf{T})$, which can be written in terms of the eigenvalues of matrix $\mathbf{I}-\mathbf{T}$, namely,

$$\det(\mathbf{I}-\mathbf{T}) = \prod_{m=1}^{5}[1-\lambda_m(\omega)]. \tag{25}$$

When the frequency ω equals a system resonance ω_i, $\det(\mathbf{I}-\mathbf{T})$ becomes zero, as shown in the previous section. The factorization is then singular because there is no transmission through specific paths but the whole system is vibrating according to one of its modal shapes. Moreover, the numerators of the weights in Eqs. (23) and (24) contain the determinants of the complementary block matrices of those masses not involved in the considered paths. For example, the numerator of the relative weight contribution for the direct path linking m_2 to m_1 (i.e., the term multiplying t_{21}) is given by $\det(\mathbf{I}-\mathbf{T}_{\{345\}})$, while that for $t_{23}t_{31}$ is $\det(\mathbf{I}-\mathbf{T}_{\{45\}})$. The numerators of the third order paths weights are unity because $\mathbf{I}-\mathbf{T}$ has ones in the diagonal, and thus coincide with the weights of fourth order paths, which have no complementary systems because, as said, they comprise all masses in the system. Next consider, for instance, the numerator of the relative weight of a second order path in Eq. (23) (there is only one of them in Eq. (24), from m_2 to m_3 and then to m_1). Such path connects three masses so the complementary block matrix is 2×2. Therefore, the numerator of the relative weight will be of the type $\det(\mathbf{I}-\mathbf{T}_{\{ij\}})$, which can be expanded as

$$\det(\mathbf{I}-\mathbf{T}_{\{ij\}}) = \prod_{m=1}^{2}[1-\lambda_{m\{ij\}}(\omega)]. \tag{26}$$

As said before, $\lambda_{m\{ij\}}(\omega)$ correspond to eigenvalues of the reduced complementary system $\mathbf{T}_{\{ij\}}$. When the frequency coincides with a resonance of the complementary system, i.e., the resonances when all other masses but m_i and m_j in the 5 dof system are blocked, $\det(\mathbf{I}-\mathbf{T}_{\{ij\}})$ becomes zero and no signal is transmitted through the path. This is logical since the masses in the path at those frequencies stand still while the complementary ones vibrate at their local resonance value.

The above explanations are illustrated for the 5 dof mechanical system in Fig. 9, where we have plotted the relative weights of the open paths connecting m_2 and m_1 in Eq. (24). As observed, all three weights $\det(\mathbf{I}-\mathbf{T}_{\{345\}})/\det(\mathbf{I}-\mathbf{T})$, $\det(\mathbf{I}-\mathbf{T}_{\{45\}})/\det(\mathbf{I}-\mathbf{T})$ and $1/\det(\mathbf{I}-\mathbf{T})$ tend to infinity at the five resonances of the system (indicated with dashed vertical lines in the figure, see Table 2) because $\det(\mathbf{I}-\mathbf{T}) = 0$ at such frequencies. Likewise, $\det(\mathbf{I}-\mathbf{T}_{\{345\}})/\det(\mathbf{I}-\mathbf{T})$ weighting the direct connection between m_2 and m_1 (first line in Eq. (24)) exhibits three drops tending to minus infinity, which correspond to the local resonances of the complementary system involving masses m_3, m_4 and m_5, where $\det(\mathbf{I}-\mathbf{T}_{\{345\}}) = 0$ (vertical green lines in Fig. 9). Analogously, $\det(\mathbf{I}-\mathbf{T}_{\{45\}})/\det(\mathbf{I}-\mathbf{T})$ weighting the second order open path from m_2 to m_3 and then to m_1, in the second line of Eq. (24), presents two drops related to the resonances of the complementary system made of m_4 and m_5 (frequencies at which $\det(\mathbf{I}-\mathbf{T}_{\{45\}}) = 0$, highlighted by blue vertical lines in the figure). Finally, the relative weight of the third order open path in the third line of Eq. (24) involves

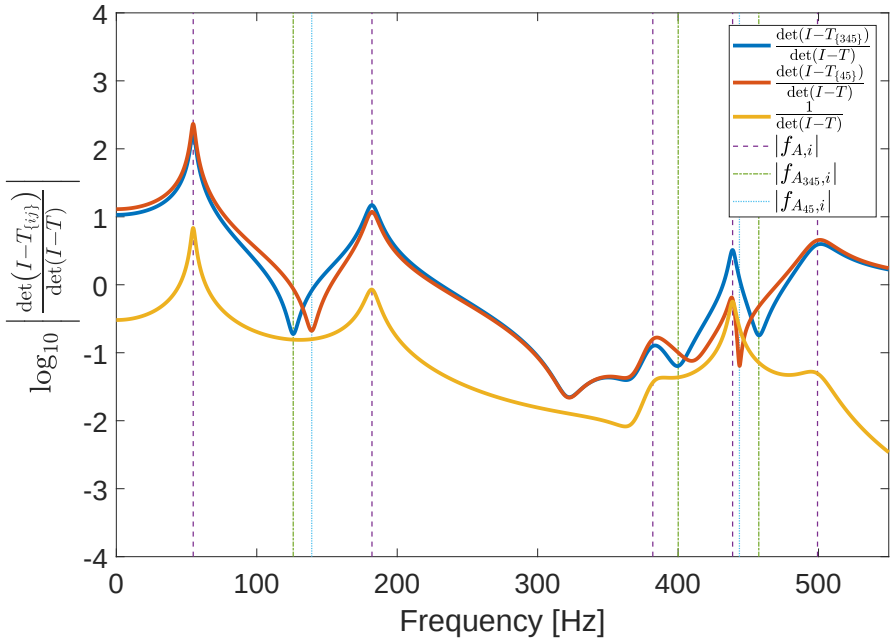

Figure 9: Modulus of the relative weights $\det(\mathbf{I}-\mathbf{T}_{\{ij\}})/\det(\mathbf{I}-\mathbf{T})$ of the open paths in Eq. (24), for the mechanical system in Fig. 6 with graph in Fig. 8.

all masses so there is no complementary system to resonate. Therefore, the relative weight never becomes zero and the logarithmic plot shows no drop for it to minus infinity. To summarize, if the system is excited at a frequency that is far from the system and complementary system resonances, the eigenvalues of $\mathbf{T}$ and $\mathbf{T}_{\{ij\}}$ are small compared to unity and Eq. (25) and Eq. (26) get close to one. Consequently, so do the relative weights in Eq. (23) and the displacement of one mass due to the displacement of another mass can be directly expanded in terms of the contributions of all open paths connecting them. The relative weights do not play a relevant role in such situation. As long as the frequency approaches a system resonance, the weights augment and become infinite when the resonance is matched. Note that the closed cycles in section 3.2 for $\det(\mathbf{I}-\mathbf{T}_{\{ij\}})$ can be therefore somehow identified with the system resonances. Besides, if the considered frequency coincides with a resonance of the complementary system of a given path, that path will transmit no signal because its weight would be negligible. This makes sense as in such situation the masses in the path remain still. The closed paths of the adjugate matrix in section 3.3 account for the influence of the resonances of the complementary systems. Interestingly, similar results were found in control theory, when analyzing the meaning of transmission zeros for lumped electro-mechanical systems. Their relation with substructure resonances was reported in [55, 56], though following a totally different argumentation neither related to graph theory nor to physical interpretation in terms of transmission paths.

4.2. Second example: a 5 subsystem SEA model

4.2.1. SEA model description

Our second example, which is representative of vibroacoustic modelling in the high frequency range, consists of an SEA model. For the ease of exposition, we also consider a simple mechanical system made of five plates that are linked together according to the sketch in Fig. 10. For simplicity, we only deal with five SEA subsystems that account for the flexural resonant modes of each plate (neither shear nor longitudinal modes

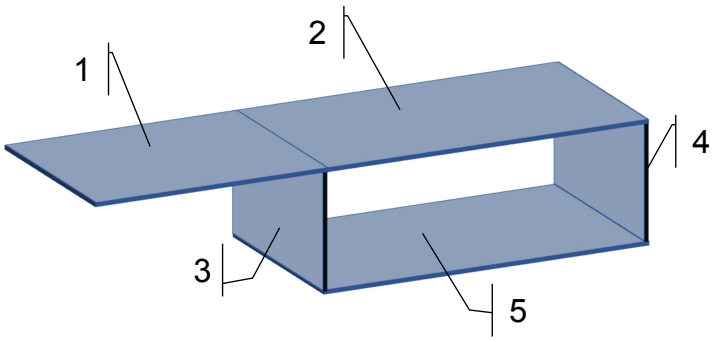

Figure 10: SEA system with the same connectivity pattern than the system in Fig. 6.

are taken into account, which are important for wave conversion at junctions see e.g., [57]). Computations have been carried out for 1/3 octave frequency bands ranging from 500 Hz to 20,000 Hz. This guarantees the number of modes per band is greater than 5. However, for the sake of brevity we will only present results for the bands centered at $f_c = \{500, 1000, 2000, 5000\}$ Hz. Besides, note that the connectivity of the plates is identical to that of the masses in the previous example of Fig. 6. Therefore, the graph in Fig. 8 will also characterize the current SEA model assigning appropriate weights to its arcs.

Matrix $\mathbf{A} \in \mathbb{R}^{5\times 5}$ is now identified with the SEA loss factor matrix,

$$A_{ij} = \begin{cases} -\eta_{ji} & i \neq j \\ \eta_i & i = j \end{cases}, \tag{27}$$

where η_{ij} designates the coupling loss factor between subsystems i and j, and η_i the total loss factor of subsystem i ($\eta_i := \eta_{id} + \sum_{i\neq j} \eta_{ij}$, with η_{id} being the damping loss factor).

The values of the SEA loss factors are provided in Table 3 and have been computed using standard SEA formulas (see e.g. [35–37]). The vector $\mathbf{x}$ in Eq.(1) contains the five subsystems energies, $\mathbf{x} = (E_1, E_2, E_3, E_4, E_5)^\top$ while vector $\mathbf{b} = (E_1^0, E_2^0, E_3^0, E_4^0, E_5^0)^\top$ is the external energy input into the system, often written as $\mathbf{b} = \omega^{-1}(W_1, W_2, W_3, W_4, W_5)^\top$, W_i being the external power input at subsystem i at the octave (or 1/3 octave) band with central frequency ω.

Making use again of $\mathbf{T} = \mathbf{I} - \mathbf{D}^{-1}\mathbf{A}$, we get the following entries for the transmissibility matrix $\mathbf{T}$,

$$T_{ij} = \begin{cases} \eta_{ji}/\eta_i & i \neq j \\ 0 & i = j \end{cases}. \tag{28}$$

In SEA, $\mathbf{T}$ directly acts as the generating matrix of the Neumann series in Eq.(4) (see [39–41]).

4.2.2. Relation between the eigenvalues of the SEA loss factor matrix and the eigenvalues of $\mathbf{T}$

As for the mass-damping-stiffness example, prior to proceeding with the path analysis, let us make some general observations on the eigenvalues of the loss factor and transmissibility matrices. Consider again the eigenpairs $(\lambda_i, \mathbf{\Phi}_i)$ of $\mathbf{T}$ satisfying $\mathbf{T}(\omega)\Phi_i = \lambda_i \Phi_i$. Note that $\lambda_i \in \mathbb{C}$ and $\Phi_i \in \mathbb{C}^{n\times 1}$ because $\mathbf{T}$ is now real but still non-symmetric. In an SEA system whose subsystems all have non-zero damping loss factor (which will be the case in any realistic model), it is easy to prove that the summation of any column of $\mathbf{T}$ is smaller than unity, i.e., $R_j := \sum_i (\eta_{ji}/\eta_j) < 1 \; \forall \; j$ (see e.g. [37]). The Gershgorin circle theorem then implies

Table 3: Total loss factors (η_i) and coupling loss factors (η_{ij}) for the SEA plate example at the 1/3 octave bands centered at $f_c = \{500, 1000, 2000, 5000\}$ Hz.

	500 Hz	**1000 Hz**	**2000 Hz**	**5000 Hz**
η_{11}	0.0790	0.0705	0.0645	0.0592
η_{21}	0.0100	0.0071	0.0050	0.0032
η_{31}	0.0231	0.0163	0.0115	0.0073
η_{12}	0.0179	0.0126	0.0089	0.0057
η_{22}	0.0764	0.0687	0.0632	0.0584
η_{32}	0.0268	0.0189	0.0134	0.0085
η_{42}	0.0398	0.0282	0.0199	0.0126
η_{13}	0.0111	0.0078	0.0055	0.0035
η_{23}	0.0061	0.0043	0.0031	0.0019
η_{33}	0.1456	0.1176	0.0978	0.0802
η_{53}	0.0136	0.0096	0.0068	0.0043
η_{24}	0.0103	0.0073	0.0051	0.0033
η_{44}	0.1223	0.1011	0.0862	0.0729
η_{54}	0.0079	0.0056	0.0039	0.0025
η_{35}	0.0457	0.0323	0.0228	0.0145
η_{45}	0.0324	0.0229	0.0162	0.0103
η_{55}	0.0715	0.0652	0.0607	0.0568

$|\lambda - T_{jj}| = |\lambda| \leq R_j < 1$, with λ being any eigenvalue of $\mathbf{T}$ (i.e., $|\lambda_i| < 1 \; \forall \; i = 1 \ldots n$). Besides, from the relation between $\mathbf{A}$ and $\mathbf{T}$ it follows that

$$\mathbf{D}^{-1}\mathbf{A}\Phi_i = (1 - \lambda_i)\Phi_i. \tag{29}$$

Given that $|\lambda_i| < 1$, $\mathbf{D}^{-1}\mathbf{A}$ will never have a null eigenvalue.

The situation for the SEA system clearly contrasts with that found for the mass-damping-stiffness example, where the eigenvalues of $\mathbf{T}$ become unity at the resonances of the system. Obviously, no global resonances are expected in SEA. Neither the eigenvalues $\lambda_m(\omega)$ of $\mathbf{T}$ in Eq.(25) nor the eigenvalues $\lambda_{m\{ij\}}(\omega)$ of the complementary systems $\mathbf{T}_{\{ij\}}$ in Eq.(26) will reach a unit value. Consequently, in SEA the physical meaning of the relative weights in the factorization Eq.(23) (see also Eq.(24)) is better explained in terms of energy transmission paths than in terms of nonexistent global and complementary system resonances. The modulus of the five eigenvalues of the plate model in Fig. 10 are plotted in Fig. 11. Although it only makes sense in SEA to present results for averaged frequency bands, in the figure we have swept the whole frequency range to confirm the mathematical prediction that all eigenvalues of $\mathbf{T}$ are smaller than one.

4.3. SEA solution in terms of transmission paths

Given that the connectivity of the SEA model in Fig. 10 coincides with that of the mass-damping-stiffness system and can be represented by the graph in Fig. 8, it follows that the factorization of the element $(\mathbf{I} - \mathbf{T})^{-1}_{21}$ of the plate model exactly matches that in Eq. (23), substituting t_{ij} by η_{ji}/η_i. It shall be noted that $(\mathbf{I} - \mathbf{T})^{-1}_{21}$ will now represent paths going from plate 1 to plate 2 (instead of going from plate 2 to 1), because loss factors appear transposed in an SEA matrix. The expansion in Eq. (23) becomes

$$\begin{aligned}
[(\mathbf{I} - \mathbf{T})^{-\mathbf{1}}]_{(2,1)} = & \frac{\det(\mathbf{I} - \mathbf{T}_{\{345\}})}{\det(\mathbf{I} - \mathbf{T})} \frac{\eta_{12}}{\eta_2} \\
& + \frac{\det(\mathbf{I} - \mathbf{T}_{\{45\}})}{\det(\mathbf{I} - \mathbf{T})} \frac{\eta_{13}}{\eta_3} \frac{\eta_{32}}{\eta_2} \\
& + \frac{1}{\det(\mathbf{I} - \mathbf{T})} \frac{\eta_{13}}{\eta_3} \frac{\eta_{35}}{\eta_5} \frac{\eta_{54}}{\eta_4} \frac{\eta_{42}}{\eta_2},
\end{aligned} \tag{30}$$

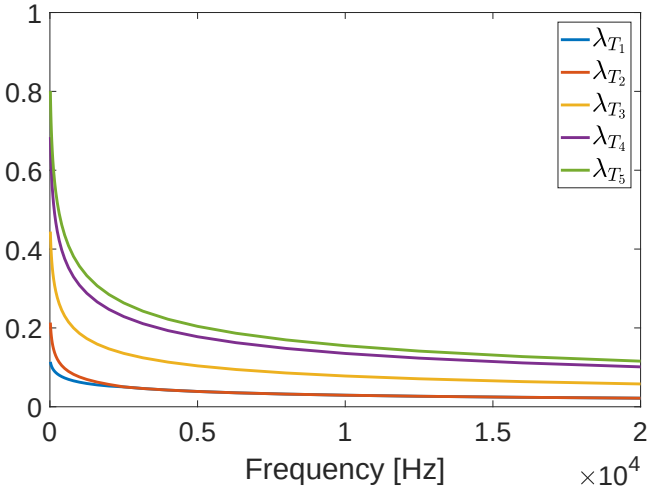

Figure 11: Eigenvalues of matrix $\mathbf{T}$ corresponding to the plate SEA system in Fig. 10.

and involves the only three existent open paths between plates 1 and 2, namely P_{12}, P_{132} and P_{13542} (see Fig. 8). The weights of P_{12}, P_{132} and P_{13542} are respectively η_{12}/η_2, $\eta_{13}\eta_{32}/\eta_3\eta_2$ and $\eta_{13}\eta_{35}\eta_{54}\eta_{42}/\eta_3\eta_5\eta_4\eta_2$, in accordance with the standard definition of SEA paths (see [38, 39, 41]). The factorization in Eq. (30) justifies the energy transmitted from plate 1 to plate 2 as contributions of the three open paths between them. These contributions must be compensated so that their overall value matches that obtained from the infinite amount of paths linking the two plates (see [39, 41]). This is the role of the relative weights $\det(\mathbf{I}-\mathbf{T}_{\{ij\ldots\}})/\det(\mathbf{I}-\mathbf{T})$ in the expression, which account for the influence of the complementary cycles on open paths.

The numerator of the relative weight of P_{13542} is one (third line in Eq. (30)) because all plates are involved in it and there is no complementary system. The numerator for P_{132}, namely $\det(\mathbf{I}-\mathbf{T}_{\{45\}}) = 1-\eta_{45}\eta_{54}/\eta_5\eta_4$ (second line in Eq. (30)) contains all complementary system cycles to P_{132}. The scalar 1 accounts for the product of the weights of loops from plate 4 to itself, i.e., P_{44}, and from plate 5 to itself, i.e., P_{55} (both loops have unit weight which results in an overall product weight of 1). Besides, $\eta_{45}\eta_{54}/\eta_5\eta_4$ is the weight of the other complementary cycle, namely the closed path P_{454}. As regards the open path P_{12}, its relative weight numerator has the expression $\det(\mathbf{I}-\mathbf{T}_{\{345\}}) = (1-\eta_{45}\eta_{54}/\eta_5\eta_4-\eta_{53}\eta_{35}/\eta_3\eta_5)$ (first line in Eq. (30)). Each term in it involves plates 3, 4 and 5 and we have plotted them in Fig. 12 for illustrative purposes. The scalar 1 corresponds to the product of the weight of the loops P_{33}, P_{44} and P_{55} (see Fig. 12a). The term $\eta_{45}\eta_{54}/\eta_5\eta_4$ now stands for the product of the weights of cycle P_{454} and loop P_{33} (let us denote the cycle set as $P_{454}\cup P_{33}$, see Fig. 12b). Finally, $\eta_{53}\eta_{35}/\eta_3\eta_5$ is the total weight for $P_{535}\cup P_{44}$, which is represented in Fig. 12c.

On the other hand, the denominator of the relative weights, $\det(\mathbf{I}-\mathbf{T})$, can be expanded as

$$
\begin{aligned}
&\det(\mathbf{I}-\mathbf{T}) = 1 \\
&- \frac{\eta_{12}}{\eta_2}\frac{\eta_{21}}{\eta_1} - \frac{\eta_{13}}{\eta_3}\frac{\eta_{31}}{\eta_1} - \frac{\eta_{23}}{\eta_3}\frac{\eta_{32}}{\eta_2} - \frac{\eta_{24}}{\eta_4}\frac{\eta_{42}}{\eta_2} - \frac{\eta_{35}}{\eta_5}\frac{\eta_{53}}{\eta_3} - \frac{\eta_{45}}{\eta_5}\frac{\eta_{54}}{\eta_4} \\
&+ \frac{\eta_{13}}{\eta_3}\frac{\eta_{31}}{\eta_1}\frac{\eta_{24}}{\eta_4}\frac{\eta_{42}}{\eta_2} + \frac{\eta_{12}}{\eta_2}\frac{\eta_{21}}{\eta_1}\frac{\eta_{35}}{\eta_5}\frac{\eta_{53}}{\eta_3} + \frac{\eta_{12}}{\eta_2}\frac{\eta_{21}}{\eta_1}\frac{\eta_{45}}{\eta_5}\frac{\eta_{54}}{\eta_4} + \frac{\eta_{13}}{\eta_3}\frac{\eta_{31}}{\eta_1}\frac{\eta_{45}}{\eta_5}\frac{\eta_{54}}{\eta_4} + \frac{\eta_{23}}{\eta_3}\frac{\eta_{32}}{\eta_2}\frac{\eta_{45}}{\eta_5}\frac{\eta_{54}}{\eta_4} + \frac{\eta_{24}}{\eta_4}\frac{\eta_{42}}{\eta_2}\frac{\eta_{35}}{\eta_5}\frac{\eta_{53}}{\eta_3} \\
&- \frac{\eta_{12}}{\eta_2}\frac{\eta_{23}}{\eta_3}\frac{\eta_{31}}{\eta_1} - \frac{\eta_{13}}{\eta_3}\frac{\eta_{32}}{\eta_2}\frac{\eta_{21}}{\eta_1} \\
&+ \frac{\eta_{12}}{\eta_2}\frac{\eta_{23}}{\eta_3}\frac{\eta_{31}}{\eta_1}\frac{\eta_{45}}{\eta_5}\frac{\eta_{54}}{\eta_4} + \frac{\eta_{13}}{\eta_3}\frac{\eta_{32}}{\eta_2}\frac{\eta_{21}}{\eta_1}\frac{\eta_{45}}{\eta_5}\frac{\eta_{54}}{\eta_4} \\
&- \frac{\eta_{23}}{\eta_3}\frac{\eta_{35}}{\eta_5}\frac{\eta_{54}}{\eta_4}\frac{\eta_{42}}{\eta_2} - \frac{\eta_{24}}{\eta_4}\frac{\eta_{45}}{\eta_5}\frac{\eta_{53}}{\eta_3}\frac{\eta_{32}}{\eta_2} \\
&- \frac{\eta_{12}}{\eta_2}\frac{\eta_{24}}{\eta_4}\frac{\eta_{45}}{\eta_5}\frac{\eta_{53}}{\eta_3}\frac{\eta_{31}}{\eta_1} - \frac{\eta_{13}}{\eta_3}\frac{\eta_{35}}{\eta_5}\frac{\eta_{54}}{\eta_4}\frac{\eta_{42}}{\eta_2}\frac{\eta_{21}}{\eta_1}.
\end{aligned}
\tag{31}
$$

This contains all cycles in the graph of Fig. 8, associated to the SEA model in Fig. 10. For instance, the unit scalar in the first line of Eq. (31) is the weight of the cycle set $P_{11} \cup P_{22} \cup P_{33} \cup P_{44} \cup P_{55}$. The second line of Eq. (31) comprises sets made of three loops and a second order closed path. The first term in this line, for example, is the weight of the cycle set $P_{121} \cup P_{33} \cup P_{44} \cup P_{55}$. In the third line of Eq. (31) we find weights of cycle sets made of two second order closed paths and one loop, such as $P_{131} \cup P_{242} \cup P_{55}$. The fourth line exposes combinations of third order closed paths and two loops, e.g., $P_{1231} \cup P_{44} \cup P_{55}$. Likewise, in the fifth line we find cycle sets built from the combination of a third order closed path and a second order one, as $P_{1231} \cup P_{454}$. The sixth line of Eq. (31) contains the weights of fourth-order paths plus one loop, like $P_{23542} \cup P_{11}$. Finally, the seventh and last line presents the weights of the two cycles visiting all plates in the graph, namely P_{124531} and P_{134531}.

In Fig. 13, we compare the energy contributions of the open paths with relative weights, with that of an infinite summation of standard SEA paths admitting cycles. The latter have been computed using the algorithm for ranking dominant energy transmission paths in [41]. Results are presented for the 1/3 octave bands with central frequencies $f_c = \{500, 1000, 2000, 5000\}$ Hz, when unit external energy is input into plate 1 in Fig. 10. At each band, Fig. 13 plots the cumulative energy level at plate 2 when increasing the number of paths. As expected, once considered all three weighted open paths the total energy at plate 2 is recovered (dashed horizontal lines in Figs. 13a-d), while for standard SEA paths one can only expect an asymptotic approach to it. To reach 99% of the energy of plate 2 at the band of 500 Hz we require 34 different paths, while 14, 8 and 5 paths are respectively needed for the bands centered at 1000 Hz, 2000 Hz and 5000 Hz.

All paths except the three open ones contain cycles (i.e., at least some plates are visited more than once), so one could understand the relative weights as some way of packaging all information on cycles and assign it to open paths. Note that if the eigenvalues of the SEA matrices $\mathbf{T}$ and $\mathbf{T}_{\{ij\}}$ were such that $\lambda_m(\omega_c) \ll 1$

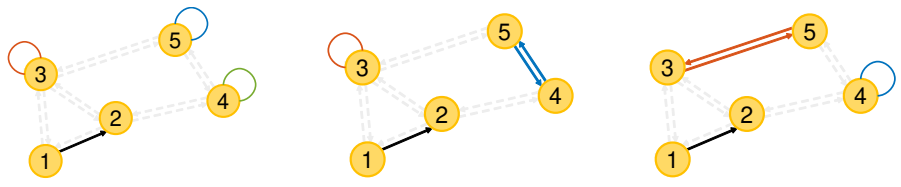

(a) (b) (c)

Figure 12: Graphs corresponding to the three terms in the numerator $\det(\mathbf{I}-\mathbf{T}_{\{345\}})$ of the relative weight for the open path P_{12}: a) $P_{33} \cup P_{44} \cup P_{55}$, b) $P_{454} \cup P_{33}$ and c) $P_{535} \cup P_{44}$.

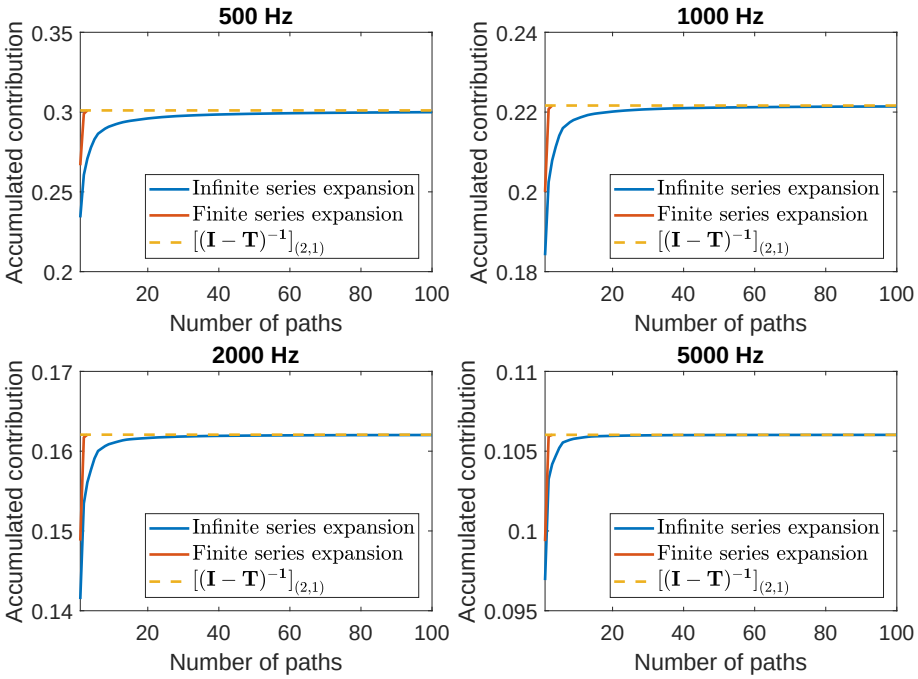

Figure 13: Cumulative contribution of weighted open paths and paths with cycles to the total energy of plate 2, when exciting plate 1, for the 1/3 octave bands centered at $f_c = \{500, 1000, 2000, 5000\}$ Hz.

and $\lambda_{m\{ij\}}(\omega_c) \ll 1$, $\omega_c = 2\pi f_c$, all weights would equal unity and the energy at a subsystem could be practically recovered from the summation of non-weighted open paths. The factorization in terms of open paths could provide a quick way to try to detect and remedy vibroacoustic problems in SEA models. It can be viewed as an alternative, or complement, of other proposed path analysis strategies [41, 42, 45].

5. Conclusions

The vibroacoustic behavior of many structures can be modelled by means of linear systems of equations. While it is known that the solution to the latter can be expanded as *infinite* series of paths connecting input degrees of freedom to target ones, in this work we have proved that it is also possible to obtain the system solution as a *finite* summation of paths. To prove this assertion, we have exploited the connection between matrix algebra and graph theory. The components in Leibniz formula for the determinant of a matrix have been interpreted in terms of open and closed paths in a graph. This has allowed us to express any element in the inverse of a matrix as a finite summation of weighted open paths connecting its two indices.

The above result is totally general and applies to any square invertible real or complex matrix, so we can consider it for the transmissibility matrix of a linear vibroacoustic system. For better understanding its physical meaning, we have addressed two representative cases of low and high vibration modelling. First, we have dealt with finite path analysis in a 5 dof mechanical system made of masses and springs with structural damping. It has been shown that the relative weights of the open paths connecting any two masses account for the influence of the complementary masses not belonging to the path. Actually, the weights are singular at the system global resonances, where path decomposition is meaningless, and vanish at the complementary system local resonances, because the masses in the path do not move at such frequencies. Providing a physical

explanation for the finite path factorization of low frequency vibroacoustic systems is one of the significant outcomes of this work, given that the infinite one is hard to interpret. In some sense, the contribution of the infinite number of loops involving complementary dofs in the infinite series expansion has been reinterpreted as the complementary system resonances in the weights of the finite one.

The second example has consisted of a statistical energy analysis (SEA) model for a set of five connected plates. It has been known for years that an SEA system solution can be expanded in terms of the contributions of an infinite number of energy transmission paths. The herein proposed finite SEA expansion in terms of open paths has the particularity that the information of all paths containing loops can be viewed as somewhat packaged in the relative weights of the open paths. A geometric interpretation of these weights has been given in terms of cycles of the whole SEA graph and cycles in complementary graphs containing subsystems not included in the open paths. A comparison has also been made between the finite and infinite series contributions for recovering the energy at one plate when exciting another one. It is expected that the finite factorization in this work could be useful to derive new transfer path analysis strategies, or complement current ones, for effectively addressing noise and vibration problems.

References

[1] J.S. Bendat, Solutions for the multiple input/output problem, J. Sound Vib. 44 (3) (1976) 311–325.

[2] J.S. Bendat, System identification from multiple input/output data, J. Sound Vib. 49 (3) (1976) 293–308.

[3] J. S. Bendat, A. G. Piersol, Engineering applications of correlation and spectral analysis, New York, Wiley-Interscience, 1980. 315 p. (1980).

[4] O. Guasch, F.X. Magrans, A compact formulation for conditioned spectral density function analysis by means of the LDL^H matrix factorization, J. Sound Vib. 277 (4-5) (2004) 1082–1092.

[5] K. Noumura and J. Yoshida, Method of transfer path analysis for vehicle interior sound with no excitation experiment, in: Proceedings of FISITA 2006, F2006D183, Yokohama, Japan, 2006.

[6] G. De Sitter, C. Devriendt, P. Guillaume and E. Pruyt, Operational transfer path analysis, Mech. Syst. Signal Pr. 24 (2) (2010) 416–431.

[7] P. Gajdatsy, K. Janssens, W. Desmet and H. Van der Auweraer, Application of the transmissibility concept in transfer path analysis, Mech. Syst. Signal Pr. 24 (7) (2010) 1963–1976.

[8] F.X. Magrans, Method of measuring transmission paths, J. Sound Vib. 74 (3) (1981) 311–330.

[9] W. Stahel, R.H. Van Ligten and J. Gillard, Measuring method to obtain the transmission paths and simultaneous real force contributions in a mechanical linear system, in: Technical Report No. 80.21, Lab. Acústico Italiana Keller (1980).

[10] J. Verheij, Multipath sound transfer from resiliently mounted shipboard machinery, Ph.D. thesis, Technische Physische Dienst TNO-TH, Delft, 1986.

[11] A. Thite, D. Thompson, The quantification of structure-borne transmission paths by inverse methods. Part 1: Improved singular value rejection methods, J. Sound Vib. 264 (2003) 411–431.

[12] A. Thite, D. Thompson, The quantification of structure-borne transmission paths by inverse methods. Part 2: Use of regularization techniques, J. Sound Vib. 264 (2003) 433–451.

[13] A.M.R. Ribeiro, J.M.M. Silva, N.M.M. Maia, On the generalization of the transmissibility concept, Mech. Syst. Signal Pr. 14 (1) (2000) 29–35.

[14] N.M.M. Maia, J.M.M. Silva, A.M.R. Ribeiro, The transmissibility concept in multi-degree-of-freedom systems, Mech. Syst. Signal Pr. 15 (1) (2001) 129–137.

[15] J. Mondot, B. Petersson, Characterization of structure-borne sound sources: the source descriptor and the coupling function, J. Sound Vib. 114(3) (1987) 507–518.

[16] A. Moorhouse, A. Elliott, T. Evans, In situ measurement of the blocked force of structure-borne sound sources, J. Sound Vib. 325 (2009) 679 – 685.

[17] M. van der Seijs, D. de Klerk, D. Rixen, General framework for transfer path analysis: History, theory and classification of techniques, Mech. Syst. Signal Pr. 68 (2016) 217–244.

[18] O. Guasch, F.X. Magrans, The Global Transfer Direct Transfer method applied to a finite simply supported elastic beam, J. Sound Vib. 276 (1-2) (2004) 335–359.

[19] O. Guasch, Direct transfer functions and path blocking in a discrete mechanical system, J. Sound Vib. 321 (3-5) (2009) 854–874.

[20] O. Guasch, C. García, J. Jové, P. Artís, Experimental validation of the direct transmissibility approach to classical transfer path analysis on a mechanical setup, Mech. Syst. Signal Pr. 37 (2013) 353 – 369.

[21] À. Aragonès, J. Poblet-Puig, K. Arcas, P. V. Rodríguez, F. X. Magrans, A. Rodríguez-Ferran, Experimental and numerical study of advanced transfer path analysis applied to a box prototype, Mech. Syst. Signal Pr. 114 (2019) 448–466.

[22] F.X. Magrans and P.V. Rodríguez and G.C. Cousin, Low and mid-high frequency advanced transmission path analysis, in: Proceedings of the Twelfth International Congress on Sound and Vibration ICSV12, Lisbon, Portugal.

[23] J. Jové, F. Guerville, A. Vallespín, Study of the aerodynamic contribution to the high-speed train cabin internal noise by means of hybrid FE-SEA modeling, in: Inter Noise 2010, Noise and Sustainability, June 13-16, Lisbon (Portugal).

[24] D. Thompson, G. Squicciarini, J. Zhang, I. L. Arteaga, E. Zea, M. Dittrich, E. Jansen, K. Arcas, E. Cierco, F. X. Magrans, et al., Assessment of measurement-based methods for separating wheel and track contributions to railway rolling noise, Appl. Acoust. 140 (2018) 48–62.
[25] O. Guasch, A direct transmissibility formulation for experimental statistical energy analysis with no input power measurements, J. Sound Vib. 330 (25) (2011) 6223–6236.
[26] D. Bies, S. Hamid, In situ determination of loss and coupling loss factors by the power injection method, J. Sound Vib. 70 (1980) 187–204.
[27] Z. Wang, P. Zhu, J. Zhao, Response prediction techniques and case studies of a path blocking system based on global transmissibility direct transmissibility method, Journal of Sound and Vibration 388 (2017) 363 – 388.
[28] J. Jové, O. Guasch, Direct response and force transmissibilities in the characterization of coupled structures, J. Sound Vib. 407 (2017) 1–15.
[29] X. Liao, S. Li, S.-K. Yang, J. Wang, Y. Xu, Advanced component transmission path analysis based on transmissibility matrices and blocked displacements, J. Sound Vib. 437 (2018) 242–263.
[30] Z. Wang, P. Zhu, A system response prediction approach based on global transmissibilities and its relation with transfer path analysis methods, Appl. Acoust. 123 (2017) 29 – 46.
[31] L. Maxit, J.-L. Guyader, Estimation of sea coupling loss factors using a dual formulation and fem modal information, part i: theory, J. Sound Vib. 239 (2001) 907–930.
[32] L. Maxit, J.-L. Guyader, Estimation of sea coupling loss factors using a dual formulation and fem modal information, part ii: numerical applications, J. Sound Vib. 239 (2001) 931–948.
[33] L. Maxit, K. Ege, N. Totaro, J.-L. Guyader, Non resonant transmission modelling with statistical modal energy distribution analysis, J. Sound Vib. 333 (2014) 499–519.
[34] J. Guyader, C. Boisson, C. Lesueur, Energy transmission in finite coupled plates, part i: Theory, J. Sound Vib. 81 (1982) 81–92.
[35] R. Lyon, R. DeJong, Theory and Application of Statistical Energy Analysis, RH Lyon Corp, Cambridge MA, 2nd Edition, 1998.
[36] R.J.M Craik, Sound Transmission Trough Buildings Using Statistical Energy Analysis, Gower, London, 1996.
[37] A. Le Bot, Foundation of statistical energy analysis in vibroacoustics, OUP Oxford, 2015.
[38] R.J.M. Craik, Sound transmission paths through a Statistical Energy Analysis model, Appl. Acoust. 30 (1990) 45–55.
[39] F.X. Magrans, Definition and calculation of transmission paths within a SEA framework, J. Sound Vib. 165 (2) (1993) 277–283.
[40] O. Guasch, L. Cortés, Graph theory applied to noise and vibration control in statistical energy analysis models, J. Acoust. Soc. Am. 125 (6) (2009) 3657–3672.
[41] O. Guasch, À. Aragonès, Finding the dominant energy transmission paths in statistical energy analysis, J. Sound Vib. 330 (10) (2011) 2325–2338.
[42] À. Aragonès, O. Guasch, Ranking paths in statistical energy analysis models with non-deterministic loss factors, Mech. Syst. Signal Pr. 52 (2015) 741–753.
[43] M. Avcu, A. Güney, Computation of dominant energy transmission paths for ship structure using a graph theory algorithm, Ocean Eng. 161 (2018) 136–153.
[44] Z. Shi, X. Yao, G. Wu, Y. Tian, The investigation on cabin noise control of ship structure based on SEA graph method, in: ASME 2018 37th International Conference on Ocean, Offshore and Arctic Engineering.
[45] O. Guasch, À. Aragonès, M. Janer, A graph cut strategy for transmission path problems in statistical energy analysis, Mech. Syst. Signal Pr. 30 (2012) 343–355.
[46] M. J. Mashayekhi, K. Behdinan, Analytical transmissibility based transfer path analysis for multi-energy-domain systems using four-pole parameter theory, Mech. Syst. Signal Pr. 95 (2017) 122–137.
[47] M. J. Mashayekhi, K. Behdinan, Analytical transmissibility based transfer path analysis for multi-energy-domain systems using bond graphs, J. Vib. Control 24 (2018) 2927–2937.
[48] À. Aragonès, L. Maxit, O. Guasch, A graph theory approach to identify resonant and non-resonant transmission paths in statistical modal energy distribution analysis, J. Sound Vib. 350 (2015) 91–110.
[49] À. Aragonès, O. Guasch, Conditions for transmission path analysis in energy distribution models, Mech. Syst. Signal Pr. 68 (2016) 245–251.
[50] F. X. Magrans, J. Poblet-Puig, A. Rodríguez-Ferran, The solution of linear mechanical systems in terms of path superposition, Mech. Syst. Signal Pr. 85 (2017) 111–125.
[51] F. Harary, The determinant of the adjacency matrix of a graph, SIAM Rev. 4 (1962) 202–210.
[52] D. M. Cvetkovic, M. Doob, H. Sachs, et al., Spectra of graphs, volume 10, Academic Press, New York, 1980.
[53] C. R. Hanusa, Applying a combinatorial determinant to count weighted cycle systems in a directed graph, Discrete Math. 309 (2009) 1746–1748.
[54] S.-C. Gong, G.-H. Xu, The characteristic polynomial and the matchings polynomial of a weighted oriented graph, Linear Algebra Appl. 436 (2012) 3597–3607.
[55] D. K. Miu, B. Yang, On transfer function zeros of general colocated control systems with mechanical flexibilities, J. Dyn. Sys. Meas. Control. 116 (1994) 151–154.
[56] G. Calafiore, S. Carabelli, B. Bona, Structural interpretation of transmission zeros for matrix second-order systems, Automatica 33 (1997) 745–748.
[57] C. Hopkins, Experimental statistical energy analysis of coupled plates with wave conversion at the junction, J. Sound Vib. 322 (2009) 155–166.